Measurement ranges of these assays were 5 to 5000 KIU/mL and 1.2 to 7.8 log IU, respectively.

Liver Biopsy

Liver biopsy specimens were evaluated by a pathologist at each institution and were scored for the stage of liver fibrosis according to the classification of Desmet et al.[12] Stage of fibrosis was assessed from stage F0 (no fibrosis) to stage F4 (cirrhosis). The patients were divided into 2 categories: mild fibrosis (F0−1) and severe fibrosis (F2−4).

ITPA Expression

Total RNA was extracted from white blood cell samples of HCV patients using RNeasy Mini Kit (Qiagen, Hilden, Germany) and reverse-transcribed using ReverTra Ace (TOYOBO, Osaka, Japan) with random primers according to manufacturer's instructions. We then amplified complementary DNAs by 35 cycles of PCR in a 25-mL reaction volume containing 1× KOD-Plus buffer (0.3 mM each primer, 0.2 mM $MgSO_4$, 1 mL DNA solution, and 1 U KOD-Plus [TOYOBO Co.]). The thermal profile was initial denaturation at 98°C for 2 minutes, followed by 35 cycles of amplification (denaturation at 98°C for 15 seconds, annealing at 58°C for 15 seconds, and extension at 68°C for 60 seconds). Nucleotide sequences of the amplified complementary DNA fragments were confirmed by direct sequencing. Real-time quantitative PCR was performed employing an ABI PRISM 7100 (Applied Biosystems) with the SYBR Green PCR Master Mix Kit (Applied Biosystems) according to manufacturer's instructions. The housekeeping gene glyceraldehyde-3-phosphate dehydrogenase was used as an internal standard.

Statistical Analysis

After GWAS-1 quality control, a linear regression model was used to test for an association between SNP genotype and Hb decline, where an additive effect of genotype was assumed. The inflation factor was estimated by the genomic control method. Multivariate logistic regression analysis with stepwise forward selection was performed with $P < .05$ as the criteria for model inclusion using the StatFlex 5.0 software package (Artec Inc, Osaka, Japan).

Results

Genome-Wide Association Analysis and Replication Study

A total of 510,537 SNPs passed quality-control filters. During the quality-control check, 11 samples suggesting kinship or sample duplication were excluded from the analysis according to PI_HAT value. The threshold for genome-wide significant association was set at $P < 9.8 \times 10^{-8}$ (.05/510,537). The genomic distribution of SNP associations is shown in Supplementary Figure

Table 2. Genome-Wide Association Study of Hemoglobin Decline at Week 4

	Set	GWAS-1			GWAS-2			Replication-1			Combined		
	Genotype	CC	CA	AA	CC	CA	AA	CC	CA	AA	CC	CA	AA
rs6051639[d] (C/A)[c]	n	108	229	116	44	111	57	68	117	73	220	457	246
	Hb decline at 4 week, g/dl	−2.48 (1.64)	−1.91 (1.44)	−1.49 (1.38)	−2.44 (1.63)	−2.10 (1.52)	−1.34 (1.64)	−2.39 (1.76)	−1.81 (1.57)	−1.31 (1.35)	−2.48 (1.63)	−1.95 (1.48)	−1.43 (1.44)
	P value[a]		4.5×10^{-7}			1.5×10^{-4}			2.0×10^{-5}			6.0×10^{-14}	
	r[b]		0.24			0.26			0.26			0.24	
rs1127354[e] (C/A)[c]	n	337	108	8	164	43	5	192	62	4	693	213	17
	Hb decline at 4 week, g/dl	−2.40 (1.45)	−0.80 (0.87)	0.20 (1.38)	−2.39 (1.48)	−0.69 (1.32)	0.07 (0.95)	−2.22 (1.62)	−0.73 (0.93)	−0.10 (1.18)	−2.34 (1.50)	−0.78 (0.99)	−0.19 (1.12)
	P value[a]		7.5×10^{-26}			2.2×10^{-11}			5.6×10^{-11}			3.5×10^{-44}	
	r[b]		0.47			0.44			0.39			0.44	

NOTE. Data given for continuous variables are mean (standard deviation) unless otherwise stated.
[a]*P* value by linear regression testing.
[b]Pearson's correlation coefficient representing the effect of a minor allele on the trait.
[c](Major/minor) allele in Japanese population.
[d]The top single nucleotide polymorphism in the genome-wide association study (GWAS) screening.
[e]Missense variant in the inosine triphosphate pyrophosphatase gene.

1*A*. The quantile−quantile plot demonstrated that several SNPs showed a stronger association than would be expected by chance, but were not significant (Supplementary Figure 1*B*), with a genomic inflation factor of 1.005. SNPs with $1.6 \times 10^{-7} \leq P < 1.0 < 10^{-5}$ were considered suggestive and retained for follow-up in the second stage. Of 49 SNPs taken forward into GWAS-2, only 1 SNP, rs6051639, located in the DDRGK1 gene on chromosome 20 (20p13 region), was found to be strongly associated with treatment-induced Hb reduction, based on the Bonferroni threshold by replication method. This association was validated in Replication-1 (Table 2).

Resequencing and Fine-Mapping

We resequenced the region surrounding the top SNP rs6051639 associated with treatment-related anemia. A recent study has reported that a missense variant in the ITPA gene affects ribavirin-induced anemia.[8] ITPA and DDRGK1 are adjacent on chromosome 20; therefore, although the LD block spans about 3 kb (Figure 1), we resequenced an approximately 37-kb genomic region encompassing DDRGK1 and ITPA loci and identified 83 common variants with minor allele frequency >0.05, 6 of which were novel (Supplementary Table 1). Of these, we genotyped as many nonredundant SNPs as possible. Four SNPs, including rs1127354, were significantly associated with ribavirin-induced anemia and in almost absolute LD with each other (Figure 1). The combined analyses of the screening and replication studies demonstrated a highly significant combined *P* value for rs1127354 (Table 2). In contrast to the considerable association found for Hb decline, baseline Hb level was not correlated with SNP (Figure 2). A significantly larger proportion of patients with the rs1127354 A allele completed treatment without ribavirin dose reduction compared to those homozygous

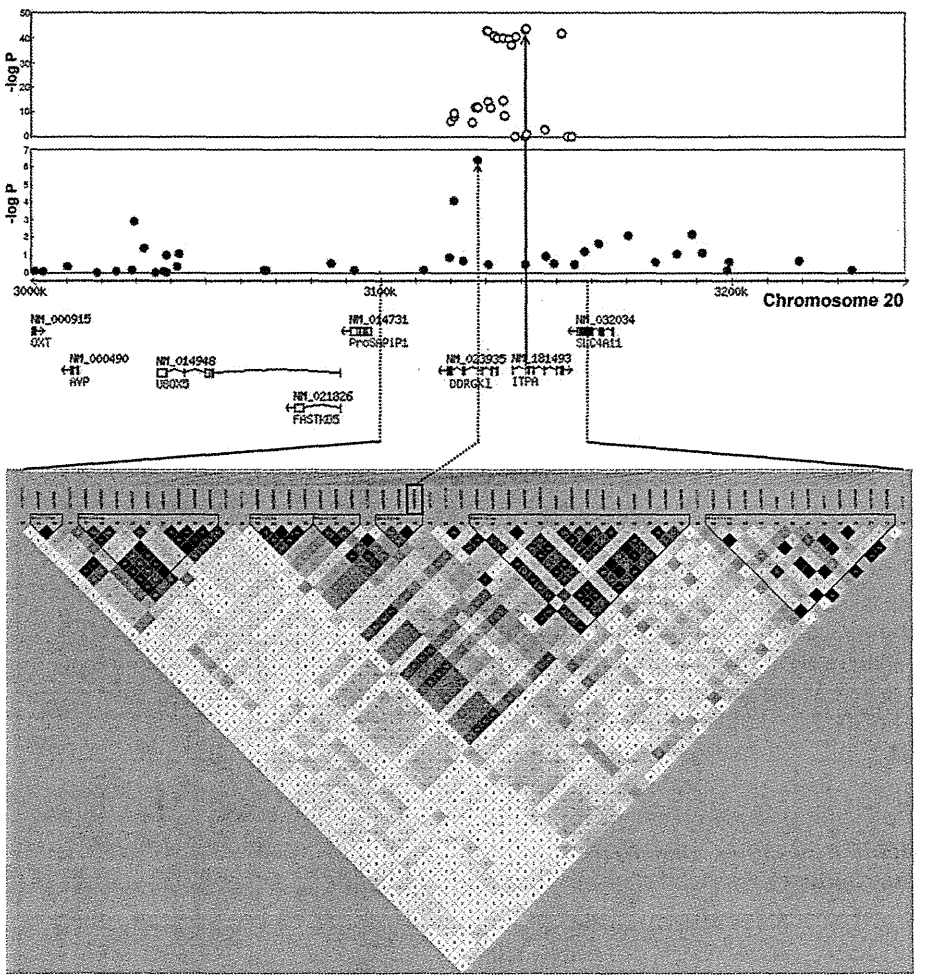

Figure 1. Depiction of the haplotype structure around the top locus. *P* value plots in linear regression analysis in genome-wide association study (GWAS)-1 stage (*middle panel*), fine-mapping using GWAS-1, GWAS-2, and Replication-1 samples (*upper panel*), and linkage disequilibrium (LD) map around DDRGK1 and inosine triphosphate pyrophosphatase (ITPA) using HapMap JPT datasets. *Dark gray:* regions with high r^2 values, *light gray:* regions with low r^2 values (*lower panel*). *Dashed line* and *arrow* represent the top single nucleotide polymorphism (SNP) rs6051639 identified by GWAS. The *solid line* and *arrow* represent the missense variant rs1127354 in the *ITPA* gene.

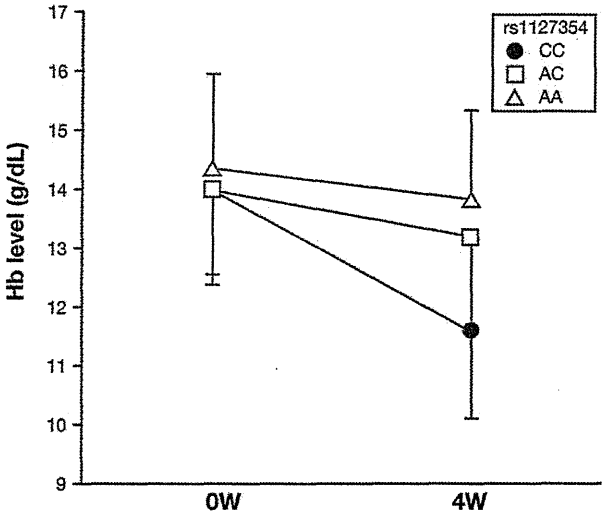

Figure 2. Inosine triphosphate pyrophosphatase (ITPA) variants and hemoglobin (Hb) level at baseline and 4-week. All the samples enrolled in the present study were stratified based on rs1127354 genotype. Markers represent means and each error bar represents 1 standard deviation.

for the C allele (rs1127354 AA/CA (83%) vs CC (37%); $P <$ .01), suggesting that the A allele is protective.

ITPA Expression Level and Ribavirin-Induced Hb Decline

Real-time quantitative PCR assays revealed no correlation between ITPA expression level and ribavirin-induced Hb decline in white blood cells. Even in stratified analysis based on the missense SNP rs1127354 genotype, we still found no correlation (Figure 3). Furthermore, we evaluated the association between ITPA expression for each SNP in the block we genotyped and found no SNPs associated with ITPA expression (data not shown).

Variables Associated With Severe Anemia

To examine the influence of potentially important prognostic factors on severe anemia (Hb <10 g/dL) necessitating dose reduction or drug withdrawal, 5 factors including known risk factors (age, sex, baseline Hb level, baseline platelet count, and rs1127354) were first examined individually by univariate logistic regression on each factor for 893 patients from the GWAS-1, GWAS-2, and Replication-1 groups. These factors were clearly associated with severe anemia (Table 3). To assess the independence of these factors, stepwise forward multiple logistic regression analysis was performed. Except for sex, all variables that were significant under univariate analyses remained significant in the final multivariate model (Table 3).

Variables Associated With Treatment Outcomes

To evaluate whether the ITPA variant affects treatment outcomes, logistic regression was used to analyze data from 522 patients who completed the therapy program with >75% compliance with prescribed doses of PEG-IFN and ribavirin. Patients were classified into the following 2 groups based on treatment outcomes: sustained viral responder and nonresponder. Sustained viral responders had no evidence of viremia at 24 weeks after completion of interferon therapy, whereas nonresponders remained viremic at this stage.

Initially 9 factors, including age, sex, BMI, baseline Hb level, baseline platelet count, fibrosis, baseline viral titer, rs1127354, and a recently reported IL-28B variant (rs8099917) genetic risk factor,[13,14] were examined individually by univariate logistic regression analysis. Individually these factors were each significantly associated with treatment outcome (Table 4). To identify independent factors, stepwise forward multiple logistic regression analysis was performed, and all variables identified by univariate analyses were retained in the final multivariate model except for baseline hemoglobin level. ITPA variant rs1127354 was retained in the final model but showed no significant association (P = .10) (Table 4).

Discussion

The anemia experienced as a consequence of PEG-IFN and ribavirin combination therapy is primarily caused by a ribavirin-induced hemolysis and secondarily by an interferon-induced bone marrow toxicity. De

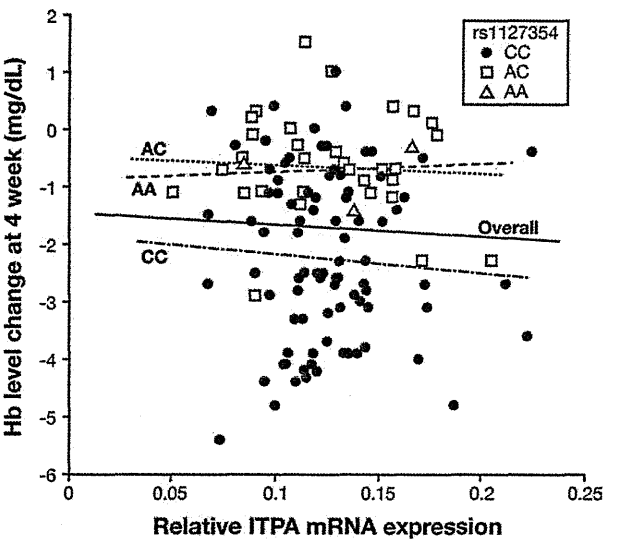

Figure 3. Inosine triphosphate pyrophosphatase (ITPA) expression level and ribavirin-induced anemia. Among genome-wide association study (GWAS)-1 and GWAS-2 patients, 124 white blood cell samples were collected and analyzed. The y-axis represents hemoglobin (Hb) level change at week 4 compared with baseline, and the x-axis represents relative messenger RNA (mRNA) expression levels of ITPA standardized by glyceraldehyde-3-phosphate dehydrogenase. The *thick solid line* represents the overall least squares best fit line and the *other 3 lines* represent best fit stratified by missense single-nucleotide polymorphism rs1127354 genotypes.

Table 3. Predictive Factors for Ribavirin-Induced Anemia in Hepatitis C Virus Patients Determined by Multivariate Logistic Regression Analysis

Variable	*P* (univariate)	*P* (multivariate)	OR	95% CI
rs1127354 (C/A)[a]	4.6×10^{-4}	1.3×10^{-4}[b]	0.20[c]	0.092–0.46
Age	.00012	.06	1.03[d]	1.00–1.05
Sex	.0065	—		
Baseline platelet count	1.0×10^{-6}	.015	0.92[e]	0.87–0.97
Baseline Hb level (*g/dL*)	2.4×10^{-14}	2.4×10^{-11}	0.56[f]	0.48–0.67

CI, confidence interval; Hb, hemoglobin; OR, odds ratio.
[a](Major/minor) allele.
[b]Additive model.
[c]The per-minor allele OR for ribavirin-induced anemia.
[d]Per year increase.
[e]Per 10^4 platelet count increase.
[f]Per g/dL hemoglobin increase.

Franceschi et al[15] proposed that the mechanism of ribavirin toxicity is that ribavirin phosphate accumulation in erythrocytes mediates oxidative damage and cell lysis. It has been reported that anemia is the major reason for dose reduction.[16] Various predictive factors for ribavirin-induced anemia have been proposed,[4–7] but it nonetheless remains difficult to predict the risk of hemolysis before administration of the drug. Haptoglobin phenotype[6] may be recognized as one of the genetic variants associated with ribavirin-induced hemolysis, although the underlying molecular mechanisms are still unknown. Recently, Fellay et al found 2 ITPA functional SNPs showing strong independent association with treatment-induced hemoglobin reduction by genome-wide association analysis.[8] Our study also identified the same missense variant in the Japanese population through genome-wide scanning followed by fine-mapping. In contrast to Fellay et al's findings, however, the splicing variant SNP rs7270101 was monoallelic in the Japanese population, and there appeared to be no other causal variants or synthetic associations with ITPA. Similarly, we found no correlation between ITPA expression and Hb decline, even after stratifying by missense variant genotypes, although examination of ITPA expression in erythrocytes or Western blot analysis of protein expression would provide additional corroborating evidence. Moreover, none of the SNPs that we genotyped in this locus was significantly associated with ITPA expression.

On the other hand, our resequencing and fine-mapping study revealed that several SNPs were in strong LD with the missense variant and were significantly associated with ribavirin-induced anemia, with *P* values varying by <1 order of magnitude. Thus, further studies are needed to identify the causal variant(s) and elucidate its functional mechanism.

Multivariate analysis demonstrated that age, baseline Hb, and rs1127354 were independently associated with severe anemia (Hb <10 g/dL) (Table 3). This finding

Table 4. Predictive Factors for Treatment Outcomes in Hepatitis C Virus Patients Treated With Peginterferon Plus Ribavirin

Variable	*P* (univariate)	*P* (multivariate)	OR	95% CI
rs1127354 (C/A)[a]	.032	.1[b]	1.4[c]	0.93–2.09
rs8099917 (T/G)[a]	4.2×10^{-10}	4.6×10^{-11}[b]	0.23[c]	0.15–0.36
Age	.000041	.004	0.97[d]	0.95–0.99
Sex	.018	.03	1.54[e]	1.04–2.27
Body mass index	.0026	.034	0.91[f]	0.86–0.98
Baseline platelet count	.000066	.017	1.05[g]	1.01–1.09
Baseline Hb level (*g/dL*)	.013	—		
Viral load (log *IU/mL*)	.00043	.00012	0.56[h]	0.42–0.75
Fibrosis (F0-2 vs F3-4)	.063	.052	0.63[i]	0.39–1.01

CI, confidence interval; Hb, hemoglobin; OR, odds ratio.
[a]Major/minor allele.
[b]Additive model.
[c]The per-minor allele OR for sustained viral response (rs1127354 AA or CA genotypes relative to CC; rs8099917 TG or GG genotypes relative to TT).
[d]Per year increase.
[e]For male patients relative to female.
[f]Per unit increase in body mass index.
[g]Per 10^4 platelet count increase.
[h]Per log viral load increase.
[i]Relative to patients with mild fibrosis (F0–F2).

suggests that rs1127354 would be a useful marker for prediction of ribavirin-induced anemia. Moreover, genetic testing of ITPA variants might be applied to establish personalized dosages in PEG-IFN and ribavirin combined therapy.

A separate multivariate analysis revealed that rs1127354 was not significantly associated with treatment outcomes, although the association was marginally significant under univariate analysis (Table 4). This might reflect decreased treatment efficacy due to dose reduction of ribavirin in patients showing severe anemia. In contrast, Fellay et al did not detect even marginal statistical significance in a similar analysis.[8] The reason for this discrepancy is unclear but may reflect a slightly higher frequency of the minor (A) (hemolysis protective) allele in the Japanese population. A similar discrepancy in the association of the ITPA variant with thiopurine intolerance between Japanese and white race has been reported.[17-19] We also found that male patients were marginally significantly more likely to respond to treatment than female patients, which may reflect the relatively high treatment age and poor response among older female patients in Japan.[20]

ITPA hydrolyses inosine triphosphate to inosine monophosphate. Several allelic variants have been described that were associated with decreased activity.[21-23] ITPA deficiency is characterized by strong accumulation of inosine triphosphate in erythrocytes.[24] A possible relationship between ITPase deficiency and adverse drug reactions to, eg, purine analogues, are documented,[19,25] although no pathological phenotypes have been found in those individuals.

Although further molecular genetic studies in relation to ribavirin-induced anemia are needed, modulation of ITPA activity might be effective to prevent severe anemia. Moreover, anti-HCV therapy in combination with an ITPA antagonist might contribute to increase sustained viral response rates by improving compliance to the therapy. On the other hand, intolerance to several therapeutic agents has been reported in patients with decreased ITPase activity.[19,25] Therefore, such combination programs should proceed but with special attention to concomitant drug administration to avoid adverse side effects.

In conclusion, we have shown that 4 polymorphisms located around the ITPA gene, including the recently reported missense variant, are strongly associated with HCV treatment-induced anemia in Japanese HCV patients. The intronic SNP, reported to affect splicing, is monoallelic in the Japanese population. Hb decline did not correlate with ITPA expression level, suggesting that the nonsynonymous SNP rs1127354 is a single causal variant associated with ribavirin-induced anemia in Japanese HCV patients. The ITPA variant can be considered to be a predictive factor for ribavirin-induced anemia in Japanese HCV patients.

Supplementary Material

Note: To access the supplementary material accompanying this article, visit the online version of *Gastroenterology* at www.gastrojournal.org, and at doi: 10.1053/j.gastro.2010.06.071.

References

1. Barrera JM, Bruguera M, Ercilla MG, et al. Persistent hepatitis C viremia after acute self-limiting posttransfusion hepatitis C. Hepatology 1995;21:639–644.
2. Hadziyannis SJ, Sette H Jr, Morgan TR, et al. Peginterferon-alpha2a and ribavirin combination therapy in chronic hepatitis C: a randomized study of treatment duration and ribavirin dose. Ann Intern Med 2004;140:346–355.
3. Manns MP, McHutchinson JG, Gordon SC, et al. Peginterferon alfa-2b plus ribavirin for initial treatment of chronic hepatitis C: a randomized trial. Lancet 2001;358:958–965.
4. Nomura H, Tanimoto H, Kajiwara E, et al. Factors contributing to ribavirin-induced anemia. J Gastroenterol Hepatol 2004;19:1312–1317.
5. Takaki S, Tsubota A, Hosaka T, et al. Factors contributing to ribavirin dose reduction due to anemia during interferon alfa2b and ribavirin combination therapy for chronic hepatitis C. J Gastroenterol 2004;39:668–673.
6. Van Vlierberghe H, Delanghe JR, De Vos M, et al. Factors influencing ribavirin-induced hemolysis. J Hepatol 2001;34:911–916.
7. Lindahl K, Schvarcz R, Bruchfeld A, et al. Evidence that plasma concentration rather than dose per kilogram body weight predicts ribavirin-induced anaemia. J Viral Hepat 2004;11:84–87.
8. Fellay J, Thompson AJ, Ge D, et al. ITPA gene variants protect against anaemia in patients treated for chronic hepatitis C. Nature 2010;464:405–408.
9. Ohnishi Y, Tanaka T, Ozaki K, et al. A high-throughput SNP typing system for genome-wide association studies. J Hum Genet 2001;46:471–477.
10. Suzuki A, Yamada R, Chang X, et al. Functional haplotypes of PADI4, encoding citrullinating enzyme peptidylarginine deiminase 4, are associated with rheumatoid arthritis. Nat Genet 2003;34:395–402.
11. Gabriel SB, Schaffner SF, Nguyen H, et al. The structure of haplotype blocks in the human genome. Science 2002;296:2225–2229.
12. Desmet VJ, Gerber M, Hoofnagle JH, et al. Classification of chronic hepatitis: grading and staging. Hepatology 1994;19:1513–1520.
13. Ge D, Fellay J, Thompson AJ, et al. Genetic variation in IL28B predicts hepatitis C treatment-induced viral clearance. Nature 2009;461:399–401.
14. Tanaka Y, Nishida N, Sugiyama M, et al. Genome-wide association of IL28B with response to pegylated interferon-alpha and ribavirin therapy for chronic hepatitis C. Nat Genet 2009;41:1105–1109.
15. De Franceschi L, Fattovich G, Turrini F, et al. Hemolytic anemia induced by ribavirin therapy in patients with chronic hepatitis C virus infection: role of membrane oxidative damage. Hepatology 2000;31:997–1004.
16. Fried MW, Shiffman ML, Reddy R, et al. Peginterferon alfa-2a plus ribavirin for chronic hepatitis C virus infection. N Engl J Med 2002;347:975–982.
17. van Dieren JM, van Vuuren AJ, Kusters JG, et al. ITPA genotyping is not predictive for development of side effects in AZA treated inflammatory bowel disease patients. Gut 2005;54:1664.

18. Gearry RB, Roberts RL, Barclay ML, et al. Lack of association between the ITPA 94C>A polymorphism and adverse effects from azathioprine. Pharmacogenetics 2004;14:779–781.
19. Uchiyama K, Nakamura M, Kubota T, et al. Thiopurine S-methyltransferase and inosine triphosphate pyrophosphohydrolase genes in Japanese patients with inflammatory bowel disease in whom adverse drug reactions were induced by azathioprine/6-mercaptopurine treatment. J Gastroenterol 2009;44:197–203.
20. Sezaki H, Suzuki F, Kawamura Y, et al. Poor response to pegylated interferon and ribavirin in older women infected with hepatitis C virus of genotype 1b in high viral loads. Dig Dis Sci 2009;54:1317–1324.
21. Sumi S, Marinaki AM, Arenas M, et al. Genetic basis of inosine triphosphate pyrophosphohydrolase deficiency. Hum Genet 2002; 111:360–367.
22. Cao H, Hegele RA. DNA polymorphisms in ITPA including basis of inosine triphosphatase deficiency. J Hum Genet 2002;47:620–622.
23. Arenas M, Duley J, Sumi S, et al. The ITPA c.94C>A and g.IVS2+21A>C sequence variants contribute to missplicing of the ITPA gene. Biochim Biophys Acta 2007;1772:96–102.
24. Vanderheiden BS. Genetic studies of human erythrocyte inosine triphosphatase. Biochem Genet 1969;3:289–297.
25. von Ahsen N, Armstrong VW, Behrens C, et al. Association of inosine triphosphatase 94CNA and thiopurine-methyltransferase deficiency with adverse events and study drop-outs under azathioprine therapy in a prospective Crohn disease study. Clin Chem 2005;51:2282–2288.

Received April 24, 2010. Accepted June 30, 2010.

Reprint requests

Address requests for reprints to: Kazuaki Chayama, MD, PhD, Department of Medical and Molecular Science, Division of Frontier Medical Science, Programs for Biomedical Research Graduate School of Biomedical Science, Hiroshima University, 1-2-3 Kasumi, Minami-ku, Hiroshima 734-8551, Japan. e-mail: chayama@hiroshima-u.ac.jp; fax: (81) 82-255-6220.

Acknowledgments

The authors thank the patients who agreed to participate in this study. We also thank the team members at Toranomon Hospital, Hiroshima University Hospital, and Hiroshima Liver Study Group for clinical sample collection. We thank T. Yokogi, H. Ishino, and K. Izumoto, T. Takajyo, and J. Sakamiya for technical assistance; and other members of the RIKEN Center for Genomic Medicine and Hiroshima University for assistance with various aspects of this study.

Conflicts of interest

The authors disclose no conflicts.

Funding

This study was supported in part by RIKEN and by Dainippon Sumitomo Pharma Co, Ltd.

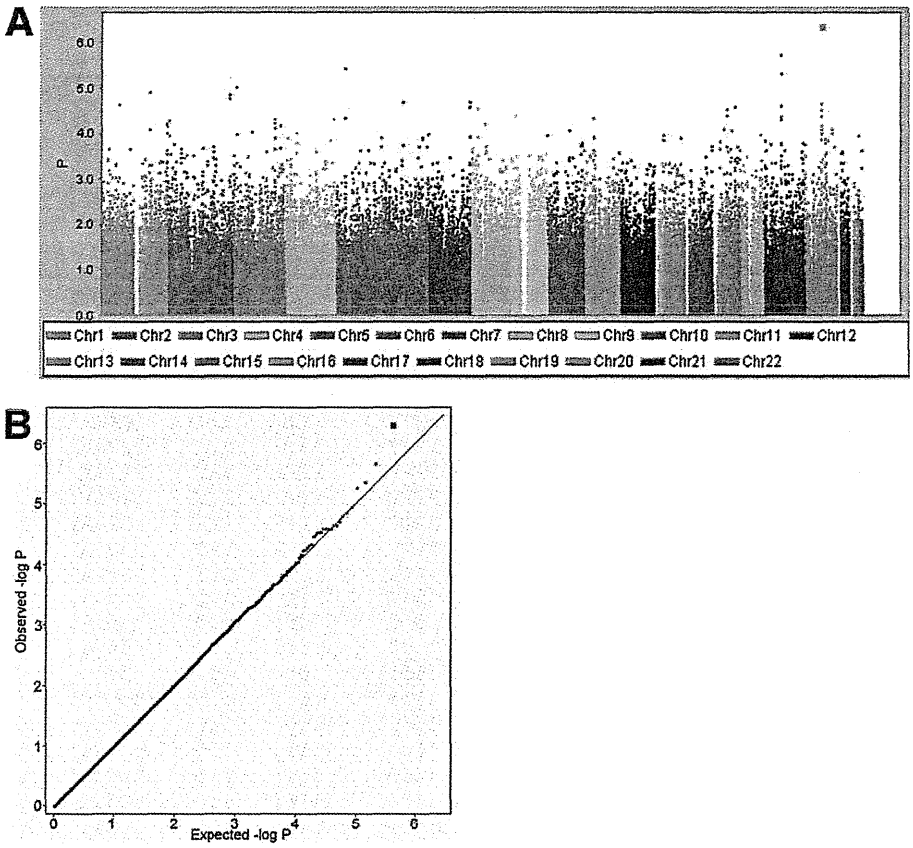

Supplementary Figure 1. Results of the genome-wide association study-1 (GWAS-1). (*A*) log10 *P* value plot at the first stage. Each *P* value was calculated by linear regression. The *large dot* corresponds to the single nucleotide polymorphism (SNP) with the strongest association, located in the DDRGK1 gene. (*B*) Quantile-quantile plot for GWAS-1. *Dots* represent *P* values of each SNP that passed the quality control filters. Only one SNP (*large dot*) in the DDRGK1 gene attained genome-wide significance after GWAS-2. The inflation factor λ was estimated to be 1.004.

Supplementary Table 1. Results of Resequencing and Fine-Mapping

SNP ID	Chr20	Allele 1	Allele 2	MAF%[a]	P(HWE)[b]	D'[c]	R^{2c}	Gene	Location	Function
—	3117545	—	T	37.2	0.3	1.00	0.11			
rs71724704	3117729	A	G	26.6	0.082	0.37	0.07			
rs71724706	3118172	C	T	24.4	0.173	0.36	0.07			
—	3118992	—	AG	21.7	0.880	1.00	0.05			
rs2295546	3119628	G	A	37.0	0.417	1.00	0.11	DDRGK1	intron9	
rs2295547	3120246	A	C	39.1	0.979	1.00	0.12	DDRGK1	intron7	
rs6051628	3120679	T	C	13.3	0.796	1.00	0.03	DDRGK1	intron6	
rs11472024	3120771	AT	—	47.7	0.555	0.77	0.11	DDRGK1	intron6	
rs6051629	3121589	C	T	46.7	0.573	0.79	0.13	DDRGK1	intron6	
rs76284374	3121710	G	A	8.7	0.518	0.66	0.23	DDRGK1	intron6	
rs8119219	3121907	T	C	37.8	0.789	1.00	0.12	DDRGK1	intron6	
rs6515773	3122105	C	T	38.0	0.681	1.00	0.12	DDRGK1	intron6	
rs7274047	3122268	C	T	38.0	0.681	1.00	0.12	DDRGK1	intron6	
rs2295548	3123260	C	T	37.8	0.789	1.00	0.12	DDRGK1	intron6	
rs2295549	3123556	G	C	46.7	0.573	0.79	0.13	DDRGK1	intron5	
rs2295550	3123694	G	A	37.8	0.789	1.00	0.12	DDRGK1	intron5	
rs2295551	3123742	A	G	37.8	0.789	1.00	0.12	DDRGK1	intron5	
rs2295552	3124009	T	C	38.9	0.903	1.00	0.13	DDRGK1	intron4	
rs7263489	3124072	C	T	32.6	0.550	1.00	0.09	DDRGK1	intron4	
rs4815575	3124443	T	A	34.4	0.663	1.00	0.11	DDRGK1	intron4	
rs6051633	3125184	A	G	35.9	0.488	0.06	0.00	DDRGK1	intron4	
rs6051634	3125188	A	G	31.5	0.329	0.18	0.00	DDRGK1	intron4	
rs6037495	3125195	C	T	29.3	0.147	0.01	0.00	DDRGK1	intron4	
rs34868732	3126817	G	A	15.2	0.941	1.00	0.03	DDRGK1	intron4	
rs6051636	3126949	C	A	47.8	0.143	0.80	0.13	DDRGK1	intron4	
rs67154167	3127366	C	A	19.6	0.246	1.00	0.05	DDRGK1	intron4	
rs6051638	3127897	T	C	46.7	0.248	0.81	0.13	DDRGK1	intron4	
rs8121983	3128226	T	C	23.9	0.0004	1.00	0.06	DDRGK1	intron4	
rs6051639	3128283	A	C	46.7	0.003	0.78	0.10	DDRGK1	intron4	
rs41281852	3128973	C	T	21.3	0.001	1.00	0.06	DDRGK1	intron3	
rs6051640	3130893	C	T	16.0	0.831	1.00	0.92	DDRGK1	intron2	
rs2326083	3131348	G	A	35.9	0.488	1.00	0.10	DDRGK1	intron2	
rs4630837	3131364	C	T	15.2	0.223	1.00	1.00	DDRGK1	intron2	
rs731282	3131404	C	T	19.6	0.823	1.00	0.05	DDRGK1	intron2	
rs2295553	3132134	T	C	46.7	0.573	1.00	0.21	DDRGK1	intron1	
rs11697186	3133123	A	T	15.2	0.223	1.00	1.00	DDRGK1	intron1	
rs6037498	3133982	C	T	16.3	0.186	1.00	0.92			
—	3134718	G	A	15.6	0.217	1.00	1.00			
rs66696167	3135609	G	A	30.7	0.543	1.00	0.08			
rs6139030	3135733	T	C	15.9	0.210	1.00	0.92			
—	3136021	T	C	4.8	0.0003	0.51	0.05			
rs6076491	3136521	G	A	17.4	0.166	1.00	0.84			
—	3136833	—	T	28.6	0.0001	0.25	0.01			
rs6051644	3137043	T	C	29.3	0.092	0.15	0.00			
rs57534080	3137091	C	T	33.7	0.150	1.00	0.09			
rs6037500	3137117	A	G	16.3	0.202	1.00	0.92			
rs6139031	3137982	G	A	16.7	0.180	1.00	0.92			
rs45620433	3138039	C	G	34.4	0.663	1.00	0.10			
rs6115814	3138790	G	T	20.0	0.852	1.00	0.05	ITPA	intron1	
rs6051646	3139068	G	A	15.6	0.217	0.73	0.54	ITPA	intron1	
rs6037501	3139205	G	T	34.1	0.552	1.00	0.09	ITPA	intron1	
rs2422860	3139464	A	G	28.4	0.739	1.00	0.08	ITPA	intron1	
rs73076878	3139725	GAA	—	50.0	1.000	1.00	0.19	ITPA	intron1	
rs59835378	3140881	A	G	30.7	0.920	1.00	0.08	ITPA	intron1	
rs6084304	3141486	C	T	48.9	0.760	1.00	0.18	ITPA	intron1	
rs6084305	3141508	T	A	47.7	0.537	0.68	0.10	ITPA	intron1	
rs11087570	3141732	G	A	17.0	0.173	1.00	0.04	ITPA	intron1	
rs1127354	3141842	C	A	15.9	0.210	—	—	ITPA	exon2	P32T
rs8362	3141978	A	G	29.5	0.401	0.24	0.00	ITPA	exon3	Q46Q
rs67002563	3142173	G	A	15.6	0.217	1.00	1.00	ITPA	intron3	
rs35991941	3142237	A	G	33.3	1.000	1.00	0.09	ITPA	intron3	
rs76430681	3142997	C	A	5.7	0.689	1.00	0.32	ITPA	intron3	
rs6076494	3143627	G	A	27.9	0.622	1.00	0.08	ITPA	intron4	

Supplementary Table 1. Continued

SNP ID	Chr20	Allele 1	Allele 2	MAF%[a]	P(HWE)[b]	D'[c]	R^{2c}	Gene	Location	Function
rs11087571	3144253	A	G	48.9	0.464	1.00	0.18	ITPA	intron5	
rs73573878	3145192	C	T	17.4	0.532	1.00	0.04	ITPA	intron5	
rs6139032	3145512	T	C	48.9	0.553	0.72	0.11	ITPA	intron5	
rs6051650	3146442	A	T	50.0	0.662	1.00	0.19	ITPA	intron5	
—	3146575	C	T	31.5	0.079	0.13	0.01	ITPA	intron5	
rs4815576	3147446	C	G	43.5	0.309	0.61	0.06	ITPA	intron6	
rs6107257	3148825	C	T	27.4	0.509	0.12	0.01	ITPA	intron6	
rs4813632	3149739	T	C	26.1	0.996	0.26	0.00	ITPA	intron6	
rs6139034	3150069	T	C	29.5	0.935	1.00	0.07	ITPA	intron6	
rs6139035	3150129	C	T	30.4	0.898	1.00	0.09	ITPA	intron6	
rs6139036	3150189	C	T	43.5	0.768	0.52	0.04	ITPA	intron6	
rs10537787	3150225	—	TGGT	29.3	0.978	1.00	0.08	ITPA	intron6	
rs6107258	3150636	G	A	19.6	0.823	1.00	0.05	ITPA	intron7	
rs66724923	3150764	A	T	48.9	0.553	1.00	0.19	ITPA	intron7	
rs2236206	3151950	A	T	30.9	0.719	1.00	0.08	ITPA	intron7	
rs9101	3152084	A	G	40.2	0.377	1.00	0.13	ITPA	exon8	E187E
rs13830	3152231	G	A	14.9	0.230	1.00	1.00	ITPA	exon8	3'UTR
rs4297961	3153008	C	T	25.0	0.024	0.00	0.00			
rs73891130	3153161	C	T	19.1	0.794	1.00	0.05			
rs6051655	3154068	G	A	19.6	0.823	1.00	0.05			

[a]Minor allele frequency.
[b]Hardy–Weinberg *P* value.
[c]The correlation coefficient with the missense single nucleotide polymorphism in the inosine triphosphate pyrophosphatase gene (rs1127354).

Journal of General Virology (2010), 91, 1668–1677 DOI 10.1099/vir.0.019315-0

Practical evaluation of a mouse with chimeric human liver model for hepatitis C virus infection using an NS3-4A protease inhibitor

Naohiro Kamiya,[1] Eiji Iwao,[1] Nobuhiko Hiraga,[2,3] Masataka Tsuge,[2,3] Michio Imamura,[2,3] Shoichi Takahashi,[2,3] Shinji Miyoshi,[4] Chise Tateno,[3,5] Katsutoshi Yoshizato[3,5] and Kazuaki Chayama[2,3]

[1]Pharmacology Department V, Mitsubishi Tanabe Pharma Corporation, Yokohama, Japan

[2]Department of Medicine and Molecular Science, Division of Frontier Medical Science, Programs for Biomedical Research, Graduate School of Biomedical Sciences, Hiroshima University, Hiroshima, Japan

[3]Liver Research Project Center, Hiroshima University, Hiroshima, Japan

[4]DMPK Department, Mitsubishi Tanabe Pharma Corporation, Kisarazu, Chiba, Japan

[5]PhoenixBio, Higashihiroshima, Japan

Correspondence
Kazuaki Chayama
chayama@hiroshima-u.ac.jp

Received 17 December 2009
Accepted 17 February 2010

A small-animal model for hepatitis C virus (HCV) infection was developed using severe combined immunodeficiency (SCID) mice encoding homozygous urokinase-type plasminogen activator (uPA) transplanted with human hepatocytes. Currently, limited information is available concerning the HCV clearance rate in the SCID mouse model and the virion production rate in engrafted hepatocytes. In this study, several cohorts of $uPA^{+/+}/SCID^{+/+}$ mice with nearly half of their livers repopulated by human hepatocytes were infected with HCV genotype 1b and used to evaluate HCV dynamics by pharmacokinetic and pharmacodynamic analyses of a specific NS3-4A protease inhibitor (telaprevir). A dose-dependent reduction in serum HCV RNA was observed. At telaprevir exposure equivalent to that in clinical studies, rapid turnover of serum HCV was also observed in this mouse model and the estimated slopes of virus decline were 0.11–0.17 $\log_{10}$ h^{-1}. During the initial phase of treatment, the $\log_{10}$ reduction level of HCV RNA was dependent on the drug concentration, which was about fourfold higher in the liver than in plasma. HCV RNA levels in the liver relative to human endogenous gene expression were correlated with serum HCV RNA levels at the end of treatment for up to 10 days. A mathematical model analysis of viral kinetics suggested that 1 g of the chimeric human liver could produce at least 10^8 virions per day, and this may be comparable to HCV production in the human liver.

INTRODUCTION

Hepatitis C virus (HCV) is a major cause for concern worldwide. More than 3 % of the world's population is chronically infected with HCV and 3–4 million people are newly infected each year (Wasley & Alter, 2000). Chronic HCV infection is relatively mild and progresses slowly; however, about 20 % of chronic hepatitis C (CHC) carriers progress to serious end-stage liver disease (Lauer & Walker, 2001; Liang *et al.*, 2000; Poynard *et al.*, 2003). The current standard treatment for HCV infection is administration of pegylated alpha interferon (PEG-IFN) in combination with ribavirin (RBV) for 48 weeks. The overall cure rates with this intervention are 40–50 % for patients with genotype 1 and more than 75 % for patients with genotypes 2 and 3 (Fried *et al.*, 2002; Manns *et al.*, 2001). Several compounds that inhibit specific stages of the virus life cycle have been clinically evaluated (Manns *et al.*, 2007; Pereira & Jacobson, 2009). Telaprevir is a novel peptidomimetic slow- and tight-binding inhibitor of HCV NS3-4A protease, which was discovered using a structure-based drug design approach (Perni *et al.*, 2006). A rapid decline in viral RNA was observed in CHC patients treated with telaprevir (Reesink *et al.*, 2006) and an increased antiviral effect of a combination of telaprevir and PEG-IFN has been reported (Forestier *et al.*, 2007). Recent clinical trials of telaprevir in combination with PEG-IFN and RBV have indicated a promising material advance in therapy for CHC patients (Hézode *et al.*, 2009; McHutchison *et al.*, 2009). First-generation HCV-specific agents have been developed despite the lack of small-animal models for HCV infection. However, early emergence of resistant variants against novel antiviral agents is a concern. Thus, the use of two or more investigation agents is strongly recommended for

clinical studies in CHC patients (Sherman *et al.*, 2007). To ensure ethical and safe clinical trials, animal models continue to be necessary for the mechanistic evaluation of the ability of specific agents to inhibit the virus life cycle *in vivo* and to develop better therapeutic strategies, including combination regimens (Boonstra *et al.*, 2009). Several groups have developed a small-animal model for HCV infection using homozygous urokinase-type plasminogen activator (uPA)/severe combined immunodeficiency (SCID) ($uPA^{+/+}$/$SCID^{+/+}$) mice transplanted with human hepatocytes (Mercer *et al.*, 2001). These mice are susceptible to cell culture-grown HCV (HCVcc; Lindenbach *et al.*, 2006) and have been used to evaluate antiviral agents including IFN-α, BILN 2061 (an NS3-4A protease inhibitor) and HCV796 (an NS5B polymerase inhibitor) (Kneteman *et al.*, 2006, 2009; Vanwolleghem *et al.*, 2007). However, the HCV clearance rate in the SCID mouse model and the virion production rate in hepatocytes engrafted in the mouse liver are not fully understood. We also generated a mouse model with an almost humanized liver (Tateno *et al.*, 2004). Using this mouse model, we reported the infection of a genetically engineered hepatitis B virus (Tsuge *et al.*, 2005) and developed a reverse genetics system for HCV genotypes 1a, 1b and 2a after intrahepatic injection of *in vitro*-transcribed RNA as well as intravenous injection of HCVcc (Hiraga *et al.*, 2007; Kimura *et al.*, 2008). In this study, we demonstrated the rapid turnover of serum HCV RNA and the pharmacokinetics (PK) and pharmacodynamics (PD) of telaprevir treatment. We concluded after quantitative estimation and the use of a mathematical model that HCV production equivalent to that in the human liver is possible in engrafted hepatocytes in this mouse model.

RESULTS

Preliminary dose-finding study

At the beginning of this study, we attempted to determine an effective dose regimen for telaprevir in this mouse model. Nine mice were randomized and treated with telaprevir over three time periods (Table 1). The lifetime kinetics of serum HCV RNA and of human serum albumin (HSA) in blood are represented in Fig. 1. One mouse (A07) exhibited a rapid reduction in HSA in the blood, which indicated the instability of human hepatocyte grafts. As a rapid reduction in HSA levels was not observed in subsequent experiments, this mouse was excluded from the mean analysis. After 7 days of twice daily (BID) dosing in period 1, the mean $\log_{10}$ changes in HCV RNA from baseline ($\pm$SEM) after the 100 and 10 mg telaprevir kg^{-1} doses were -0.49 ± 0.094 and -0.53 ± 0.039, respectively, and no dose-dependent reduction was observed. During period 2, the dose frequency was changed from BID to three times daily (TID), and the time of serum sampling was also changed from 1 to 4 h after the last dose. After the 3-day treatment, the mean $\log_{10}$ changes of HCV RNA in 100 and 10 mg telaprevir kg^{-1} TID groups were -1.00 ± 0.166 and -0.28 ± 0.056, respectively, and the difference between the two groups was significant. To test the reproducibility of results, mice were treated with 10 or 100 mg telaprevir kg^{-1} TID for 10 days and then sacrificed 5 h after the administration of the last dose. The mean $\log_{10}$ changes in serum HCV RNA were -1.46 ± 0.265 and -0.27 ± 0.073 in the 100 and 10 mg kg^{-1} TID groups, respectively, and the difference between the means was significant.

Evaluation of HCV turnover in this mouse model

Because of the SCID nature of this mouse model, the virion clearance mechanism was of interest. Six mice with steady-state and high viral loads (9.7×10^5–1.2×10^8 copies ml^{-1}) were administered 200 mg telaprevir kg^{-1} TID for 4 days, with 5 h intervals between doses and a 14 h intermission from drug treatment each day. Because the $\log_{10}$ reduction in HCV RNA appeared to depend on the time of serum collection during the day (Fig. 2a), the mean $\log_{10}$ changes in HCV RNA were plotted against time and fitted to a linear regression model (Fig. 2b). The estimated slopes (i.e. $\log_{10}$ HCV reduction per hour) and 95% confidence intervals (CI) on days 1, 2 and 3 were -0.165 (-0.268 to 0.0616), -0.115 (-0.131 to 0.0990) and -0.153, respectively. These regression lines also suggested that extrapolated HCV loads at the actual times of the daily first doses were 0.0530, -0.220 and -0.0948 $\log_{10}$ copies ml^{-1}, respectively. Therefore, it appeared that the viral load

Table 1. Telaprevir dose-finding experiment

Period	Duration (days)	Frequency of dose (per day)	Dose (mg kg^{-1})	No. of mice	Mean $\log_{10}$ changes $\pm$ SEM	*P* value (*t* test)
1	7	2	100	4	-0.49 ± 0.094	0.7806
			10	3*	-0.53 ± 0.039	
			0	1	-0.47	
2	3	3	100	4*	-1.00 ± 0.166	0.0064
			10	4	-0.28 ± 0.056	
3	10	3	100	3	-1.46 ± 0.265	0.0125
			10	3	-0.27 ± 0.073	

*One mouse was excluded because of instability of human hepatocyte grafts.

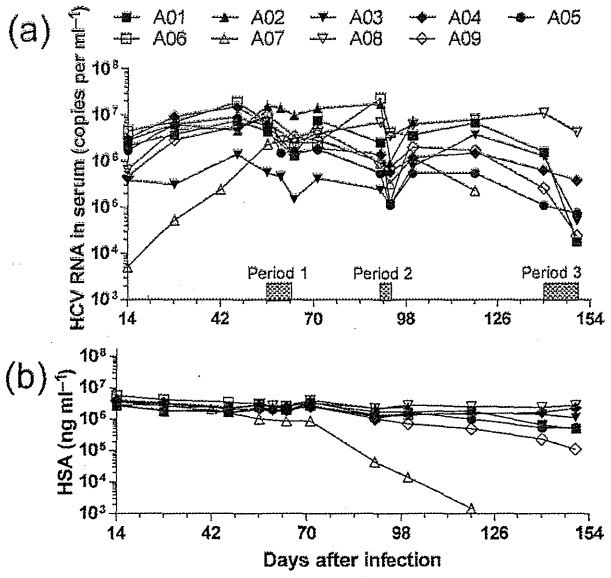

Fig. 1. Lifelong changes in serum HCV RNA and HSA in the blood of HCV-infected mice in the preliminary dose-finding experiment. Nine HCV-infected mice (A01–A09) were treated with telaprevir over three independent periods. The mice were treated with 10 mg telaprevir kg^{-1}, 100 mg telaprevir kg^{-1} or vehicle BID for 7 days (period 1), TID for 3 days (period 2) and TID for 10 days (period 3). (a) Kinetics of serum HCV RNA. (b) Kinetics of HSA level in blood. Because the HSA level indicated the stability of engrafted human hepatocytes in the mice, mouse A07 was excluded from the summary of the results in Table 1.

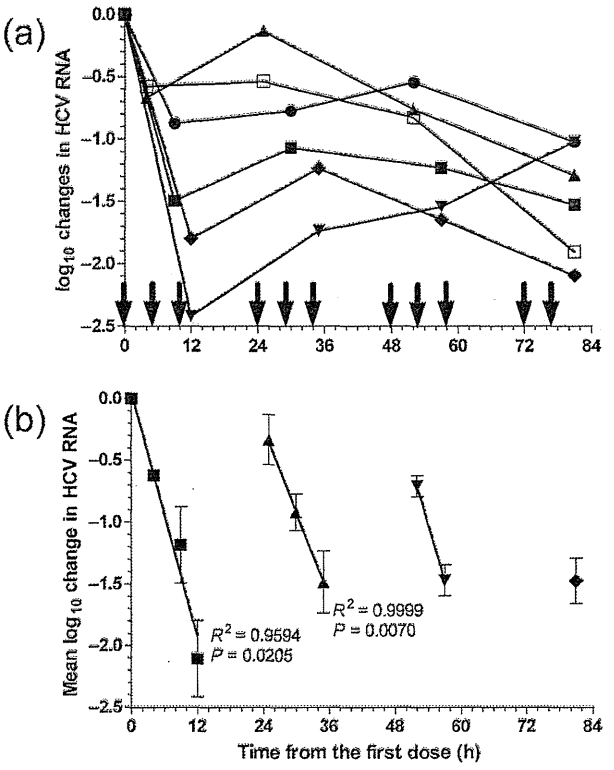

Fig. 2. Estimation of virus clearance rate. Six HCV-infected mice were treated with 200 mg telaprevir kg^{-1} TID for 4 days. Individual kinetics of $\log_{10}$ reductions in serum HCV RNA (a) and of mean $\log_{10}$ changes (± SEM) at each sampling time (b) are represented. Arrows indicate the times of dosing. The slopes of mean $\log_{10}$ HCV RNA reduction were estimated by linear regression analysis. P and R^2 values are indicated on the figure.

reverted back towards baseline levels during the 14 h intermission from drug treatment.

PK analysis

To assess drug exposure after repeated dosing in this mouse model, mice were administered 100 or 300 mg telaprevir kg^{-1} BID for 4 days. The mice receiving 300 mg kg^{-1} BID for 4 days had a mean 2 $\log_{10}$-fold HCV reduction, whereas those receiving 100 mg kg^{-1} BID had up to a 1.5 $\log_{10}$-fold reduction by day 3 (Fig. 3a). Plasma telaprevir concentrations after administration of the final dose are indicated in Fig. 3(b). The estimated half-life of telaprevir in the 100 and 300 mg kg^{-1} groups was 2.4 and 3.8 h, respectively.

PK/PD analysis and the dose-dependent reduction in HCV RNA

To evaluate the correlation between telaprevir concentration and HCV reductions in this mouse model, we used another cohort of 12 HCV-infected mice with high viral loads (1.6×10^6–3.9×10^8 copies ml^{-1}). In this crossover study, mice were randomized into three groups (n=4 each), each of which underwent two periods of dosing for 5 days separated by a 1-week washout period. Serum and plasma samples were collected once daily 5 h after dosing. The mean $\log_{10}$ changes in HCV RNA (± SEM) at different dose levels were calculated from the combined results of both periods (Fig. 4a). The mean $\log_{10}$ reductions from baseline in the 100 and 300 mg kg^{-1} groups were approximately 1 $\log_{10}$ and 1.5–2 $\log_{10}$, respectively, and the difference between the two groups was statistically significant. The means calculated in each period separately are also shown in Fig. 4(b). The plasma telaprevir concentration was positively correlated with the $\log_{10}$ HCV RNA reduction level in each period (Fig. 4c).

Drug concentrations and HCV levels in blood correlate with those in the liver

The correlation between telaprevir concentrations in the plasma and liver was analysed in a double logarithmic plot 5 (dose-finding cohort) or 8 h (PK and PK/PD cohorts) after the last dose (Fig. 5). The linear regression lines suggested that telaprevir concentrations in the liver were 5–

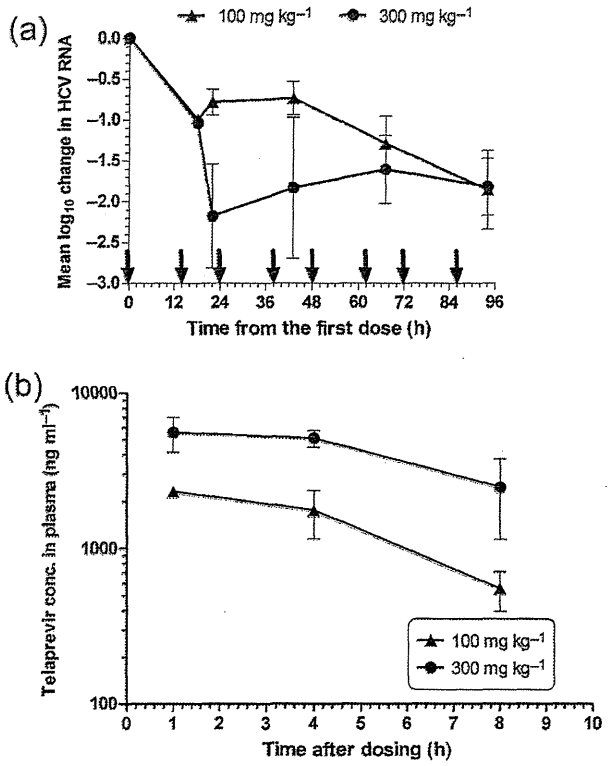

Fig. 3. PK analysis of telaprevir in the HCV-infected mouse model. Six HCV-infected mice were administered 100 (n=3) or 300 (n=3) mg telaprevir kg^{-1} BID for 4 days and serum samples were collected once daily to assess antiviral activity. After the last dose, plasma samples were collected at 1, 4 and 8 h for PK analysis. (a) Mean $\log_{10}$ changes (± SEM) in serum HCV RNA from mice treated with telaprevir. Arrows indicate the times of dosing. (b) Kinetics of telaprevir concentrations in plasma after the last dose.

10-fold higher at 5 h and approximately fourfold higher at 8 h than those in plasma. Total cellular RNA samples were extracted from two, one and four discrete small sections (approx. 50 mg) of the liver in the preliminary dose-finding, PK and PK/PD cohorts, respectively. HCV RNA levels in the total cellular RNA extract were relatively quantified by duplex real-time RT-PCR analysis using human β_2-microglobulin (hβ_2m) as an internal standard of human endogenous gene expression. Neither the threshold cycle (Ct) of hβ_2m ($Ct_{h\beta 2m}$) nor the Ct of HCV (Ct_{HCV}) correlated with total RNA from a small section of the chimeric human livers (data not shown). This result indicated that occupancy rates of human cells varied individually and/or among small sections of the chimeric human liver. Therefore, the mean difference in Ct ($\Delta Ct = Ct_{HCV} - Ct_{h\beta 2m}$) in each mouse was calculated and plotted against the viral load in serum (Fig. 6). After treatment with telaprevir for up to 10 days, mean ΔCt values ranged between 11 (HCV RNA content: $2^{11} = 2 \times 10^3$-fold lower than hβ_2m expression) and 17 (1×10^5-fold lower) among the HCV-infected mice and correlated linearly with $\log_{10}$ serum HCV RNA levels.

Viral dynamics model analysis

To evaluate time-dependent reductions in HCV with BID dosing, 12 HCV-infected elderly mice, which maintained high and steady-state viral loads (1.2×10^6–8.5×10^7 copies ml^{-1}) for more than 6 months, were treated with 200 mg telaprevir kg^{-1} BID for 3 days. The mice were divided into two groups, and serum samples were collected just before the second dose and 4 (n=6) or 8 (n=6) h after every two administrations. The single administration of telaprevir resulted in a mean 0.8–1.0 $\log_{10}$-fold reduction in HCV RNA in both groups. After the second dose, the pattern of viral kinetics appeared to depend on the time of serum collection, and the mean HCV RNA reduction level was higher in the 8 h group than in the 4 h group and plateaued at approximately a 2 $\log_{10}$-fold reduction in both groups after treatment for 3 days (Fig. 7). Finally, we attempted to estimate parameters of efficacy (ε) and virus clearance (c) per hour in this mouse model for comparison with estimates derived from human studies. Because the mean viral kinetics of the 8 h group was biphasic, the values in the 8 h group were used together for the mathematical model analysis. The estimated ε and c values were 0.992 (95 % CI 0.982–1.00) and 0.200 (95 % CI 0.110–0.291), respectively.

DISCUSSION

Using a mouse model with a chimeric human liver for HCV infection, we analysed the PK/PD of telaprevir treatment and investigated HCV dynamics during the initial phase of protease inhibitor treatment. All the mice in this study were expected to have more than half of their livers repopulated by human hepatocytes (Tateno *et al.*, 2004), which simulates a human drug metabolism profile (Katoh *et al.*, 2007, 2008). After the infection with HCV genotype 1b, high viral loads were maintained in the mice for more than 6 months. Recent studies have indicated the utility of a human/mouse chimera model for HCV infection to evaluate antiviral efficacy (Kneteman *et al.*, 2006, 2009) and preclinical safety (Vanwolleghem *et al.*, 2007). However, PK/PD studies and estimations of virus clearance rate have rarely been performed in this mouse model. HCV production, including intracellular replication in engrafted hepatocytes, has also not yet been elucidated. Despite the SCID nature of this mouse model, a 2 $\log_{10}$-fold HCV RNA reduction was observed within 0.5 days, as has been observed previously in CHC patients (Forestier *et al.*, 2007; Reesink *et al.*, 2006). In this mouse model, the rapid rebound in HCV load during the intermission from drug exposure indicated the rapid production and release of HCV into the circulation. This finding indicates that a virion-clearing compartment, which does not depend on T- and B-cell responses, may exist in this mouse model.

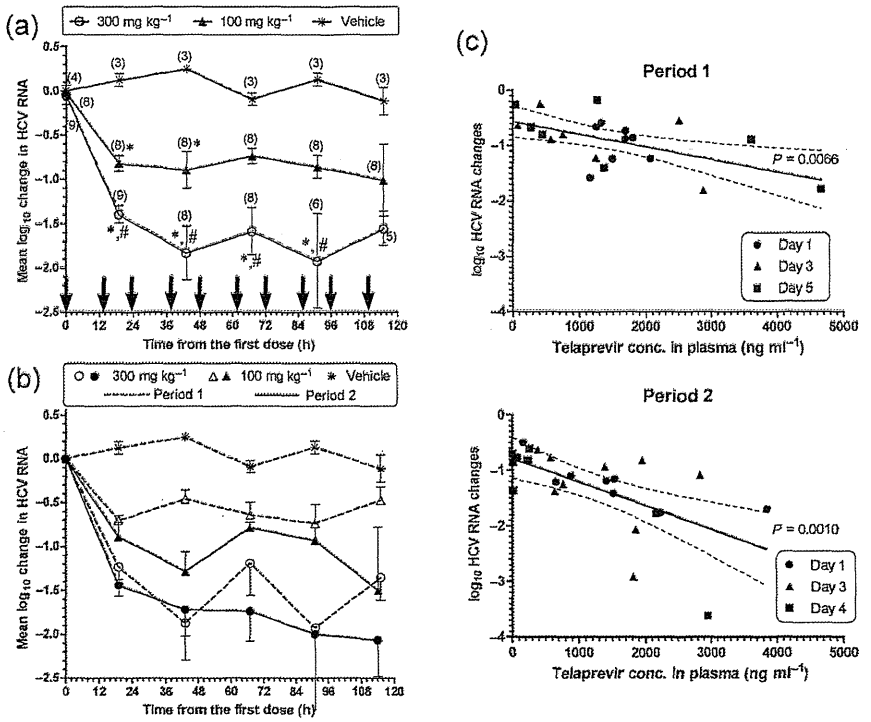

Fig. 4. PK/PD analysis and the dose-dependent reduction in HCV. Twelve HCV-infected mice were randomized into three groups (n=4 each) and then underwent two periods of telaprevir BID dosing for 5 days, separated by a 1-week washout period. Before the second period, the mice in the vehicle control group were additionally assigned to active drug groups. During the second period, mice that received the high or low doses were crossed over to the alternative treatment. Serum and plasma samples were collected once daily 5 h after dosing. Mean $\log_{10}$ changes (± SEM) in serum HCV RNA were calculated from the combined results from both periods (a) and each period separately (b). Arrows indicate the times of dosing. *, $P<0.05$ versus vehicle control group; #, $P<0.05$ versus 100 mg kg^{-1} group. (c) Correlation between $\log_{10}$ reduction in serum HCV and telaprevir concentrations in plasma. Linear regressions (solid lines) and 95 % CI (dashed lines) are indicated.

One possible explanation is that viral kinetics after liver transplantation in humans may play a role in HCV clearance under immunosuppressed conditions (Dahari *et al.*, 2005; Powers *et al.*, 2006; Schiano *et al.*, 2005). This observation suggests that this mouse model is capable of evaluating 'first-phase' HCV clearance after drug treatment.

In a clinical trial of telaprevir, CHC patients who exhibited a continuous decline in viral kinetics had mean plasma trough levels above 1000 ng ml^{-1}; therefore, a dose of 750 mg TID was selected for further clinical studies (Sarrazin *et al.*, 2007). When HCV-infected mice were administered 100 or 300 mg telaprevir kg^{-1}, a plasma concentration above 1000 ng ml^{-1} was maintained beyond 8 h in mice treated with 300 mg kg^{-1} but not in those treated with 100 mg kg^{-1}. This result suggests that the extrapolation of telaprevir doses from this mouse model to human studies depends on body surface area, i.e. approximately 15th of a dose in this mouse model may be equivalent to a dose in humans. In another cohort of mice treated with 100 and 300 mg telaprevir kg^{-1} BID, a dose-dependent reduction in HCV was observed and the plasma telaprevir concentration correlated significantly with the HCV reduction level. Therefore, the PK/PD results in this mouse model may be able to indicate a targeted dose range in clinical studies.

Whereas a telaprevir concentration in plasma equivalent to its dosage in clinical trials was achieved in this mouse model, the serum HCV RNA level plateaued at a decrease of approximately 2 $\log_{10}$-fold within several days of treatment. A saturated reduction of approximately 2 $\log_{10}$-fold after treatments with BILN 2061 and IFN was also reported in an analogous mouse model (Kneteman *et al.*, 2006; Vanwolleghem *et al.*, 2007). These observations led us to examine HCV replication in the chimeric human liver. In the relative quantification of HCV RNA against human-specific endogenous gene expression, we observed a correlation between the serum HCV RNA level and the mean ΔCt value in the liver, despite no correlation between the total RNA concentration and each Ct value of two target genes in the liver RNA extracts. This result can be interpreted to indicate that HCV replicated only in

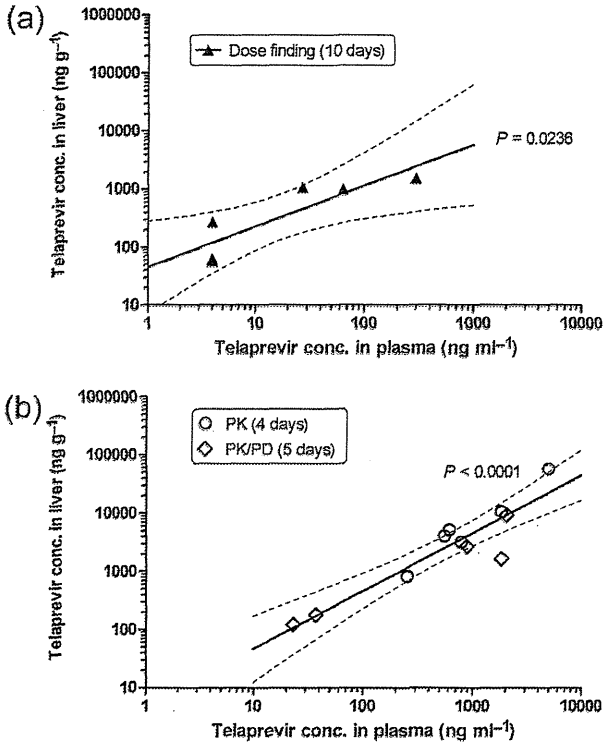

Fig. 5. Correlation between telaprevir concentrations in the liver and plasma. Telaprevir concentrations in the liver and plasma were determined at the end of the three different experiments indicated in Fig. 1 (dose-finding), Fig. 3 (PK) and Fig. 4 (PK/PD). Telaprevir concentrations in the liver were plotted against those in plasma 5 (a) or 8 (b) h after the last dose. Linear regressions (solid lines) and 95 % CI (dashed lines) are indicated.

engrafted human hepatocytes, and the observed HCV reduction in serum might reflect virus replication in the human hepatocyte grafts. Moreover, the relative content of HCV RNA was 2×10^3–1×10^5-fold lower than hβ_2m expression, whereas an HCV replicon cell line, which had approximately 1000 replicon genomes per cell (Quinkert *et al.*, 2005), contained nearly equal amounts of both genes (data not shown). HCV replication was much lower in the engrafted human hepatocytes than in an HCV replicon cell line, and HCV infected only a small portion of the engrafted human hepatocytes. It has been reported that 4–25 % of hepatocytes in a CHC patient were positive for replicative-intermediate RNA, and the mean number of viral genomes per productively infected hepatocyte ranged from 7 to 64 molecules (Chang *et al.*, 2003). Also, a more recent report suggested that the percentage of HCV antigen-positive hepatocytes in patients varied from 0 to 40 %, and the HCV content in 2000 microdissected HCV-positive cells ranged from 40 to 1800 international units using a branched DNA assay (Vona *et al.*, 2004). Therefore, we suggest that HCV replication efficiency in engrafted human hepatocytes is equivalent to that in CHC patients.

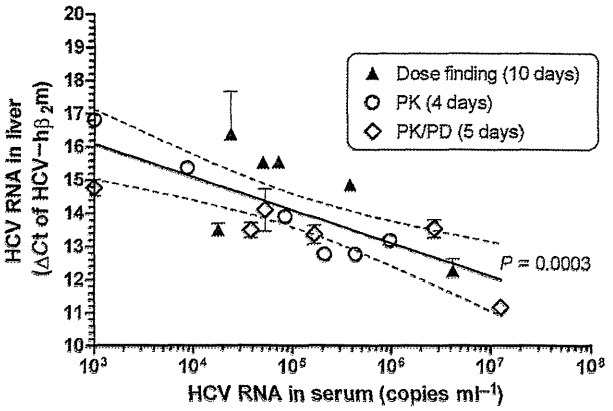

Fig. 6. Correlation between HCV content in the liver and serum. Relative quantification of HCV RNA levels in the liver was determined by the difference between threshold cycles (ΔCt) of HCV RNA and hβ_2m in a duplex real-time RT-PCR analysis. Linear regressions (solid line) and 95 % CI (dashed lines) are indicated.

The differences observed between the engrafted human hepatocytes and the HCV replicon cell line can be explained by the following assumptions: approximately 10 % of engrafted human hepatocytes are productively

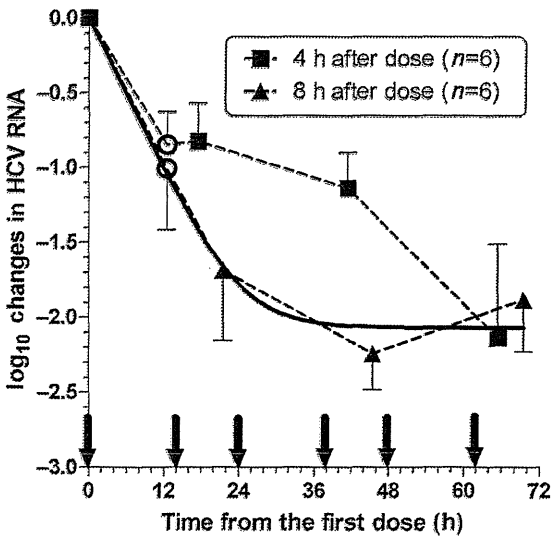

Fig. 7. Viral dynamics under BID telaprevir treatment. Mice were administered 200 mg telaprevir kg^{-1} BID at the times indicated by arrows. Serum samples were collected just before the second dose was administered and 4 (n=6) or 8 (n=6) h after every two doses were administered. Mean $\log_{10}$ changes (± SEM) in serum HCV RNA are plotted. The solved equation described in Methods was fitted to the values in the 8 h group (solid line), and the estimated efficacy and virion clearance rates were 0.992 (95 % CI 0.982–1.00) and 0.200 (95 % CI 0.110–0.291), respectively.

infected and harbour approximately ten HCV genomes per cell at baseline steady state and a 2 $\log_{10}$-fold reduction is achieved with drug treatment.

Mathematical models have proven valuable in understanding the *in vivo* dynamics of HCV, and very rapid dynamic processes occur on timescales of hours to days, and slower processes occur on timescales of weeks to months (Perelson & Ribeiro, 2008). In the last experiment, we observed a biphasic decline in the HCV RNA level after BID dosing for 3 days. During the first 2 days of the treatment, a discrepancy in viral kinetics between the serum-sampling time points was noted. Similarly, fluctuations in viral kinetics during the first-phase slope were observed in patients who received IFN three times a week (Pawlotsky *et al.*, 2004). Variable efficacy rate determined by PK parameters can explain fluctuations during the first-phase slope in mathematical model analysis (Talal *et al.*, 2006). However, it is difficult to evaluate the individual temporal changes in viral and drug kinetics using a mouse model as only a limited volume of blood is available for analysis. Therefore, we assumed a constant efficacy rate (ε) and omitted a turnover rate of hepatocytes because of the short duration of treatment. The estimated clearance rate (c) in this study was 4.8 day^{-1}. Additionally, the mean slope of 0.144 $\log_{10}$ h^{-1} (Fig. 2b) could be transformed to 0.332 h^{-1}=8.0 day^{-1} according to the change of base of a logarithm. The estimated clearance rates in this mouse model basically agreed with estimates determined in humans infected with HCV genotype 1 and undergoing IFN-based therapies (Herrmann *et al.*, 2003; Neumann *et al.*, 1998; Pawlotsky *et al.*, 2004) or large-volume plasma apheresis (Ramratnam *et al.*, 1999). Total virion production during steady-state viral kinetics in this mouse model was calculated by multiplying c by the initial viral load (V_0) and then normalizing the extracellular fluid volume. From previous studies, it was determined that 10^{11}–10^{13} virions are produced daily in patients with high HCV loads (Neumann *et al.*, 1998; Ramratnam *et al.*, 1999). In this mouse model, the volume of extracellular fluid and weight of the liver were approximately 20 and 9 % of the body weight (data not shown), and the mean $\log_{10}$ V_0 ($\pm$SEM) among the mice with mean clearance rates of 4.8 and 8.0 per day were 6.96 ± 0.26 and 7.00 ± 0.33, respectively. The results of the calculations indicated that 1 g of the chimeric human liver produced 1×10^8–2×10^8 virions per day. The typical weight of the human liver is 1–2 kg; thus, the capacity of human hepatocytes to produce HCV in this mouse model may be equivalent to that in CHC patients. In conclusion, a mouse model with a chimeric human liver can simulate HCV replication in human patients quantitatively and dynamically, and this mouse model may be suitable for preclinical evaluations of novel HCV-specific agents and other therapeutic strategies, including combination regimens.

METHODS

Generation of mice with chimeric human livers and HCV infection. The generation of uPA$^{+/+}$/SCID$^{+/+}$ mice and transplantation of frozen human hepatocytes was performed at PhoenixBio. Graft function was monitored on the basis of HSA levels in blood (Tsuge *et al.*, 2005). All the mice had high HSA levels, which suggested that nearly half of their livers were repopulated by human hepatocytes (Tateno *et al.*, 2004). After obtaining written informed consent, we collected sera periodically from patients who were chronically infected with HCV genotype 1b and failed to respond to PEG-IFN and RBV therapy. The mice were inoculated with the serum samples via the orbital vein after anaesthetization. The experimental protocol was approved by the Ethics Review Committee for Animal Experimentation of the Graduate School of Biomedical Sciences, Hiroshima University.

Compound preparation and experimental designs. The telaprevir formulations were kindly provided by Vertex Pharmaceuticals. A telaprevir suspension was prepared as described previously (Perni *et al.*, 2006) and used in experiments 1 and 2. In the other experiments, a telaprevir suspension was prepared daily as in the tablet formulation (Forestier *et al.*, 2007; Hézode *et al.*, 2009; McHutchison *et al.*, 2009). A suspension of telaprevir was administered via oral gavage.

Experiment 1: preliminary dose-finding study. Ten out of 11 mice developed serum HCV loads greater than 10^4 copies ml^{-1}. Nine mice with high viral loads (>10^5 copies ml^{-1}) were randomized and administered 10 or 100 mg telaprevir kg^{-1} BID or TID over three periods. During period 1, the mice were administered 100 (n=4) or 10 (n=4) mg telaprevir kg^{-1} or vehicle (n=1) BID at 18:00 and 10:00 h for 7 days, and serum samples were collected before treatment and 1 h after administration in the morning on the third and/or seventh day. During period 2, the mice were administered 100 (n=5) or 10 (n=4) mg telaprevir kg^{-1} TID for 3 days, and serum samples were collected before treatment and 4 h after administration of the last dose. Three mice died between periods 2 and 3. During period 3, the mice were administered 100 (n=3) or 10 (n=3) mg telaprevir kg^{-1} TID for 10 days. The mice were sacrificed 5 h after administration of the last dose, and plasma, serum and liver samples were collected.

Experiment 2: evaluation of HCV turnover. Eleven mice were infected with HCV and eight mice survived for more than 15 weeks with steady-state and high viral loads (10^6–10^8 copies ml^{-1}). Six of the mice were administered 200 mg telaprevir kg^{-1} TID at 9:00, 14:00 and 19:00 h for 4 days. On day 1, serum samples were collected before dose administration, 4 h after the first and second doses were administered, and 2 h after the third dose was administered (n=2 each). On day 2, serum samples were collected 1 h after each of the three doses was administered (n=2 each). Serum samples were also collected 4 h after the first and second doses were administered on day 3 (n=3 each) and 4 h after the second dose was administered on day 4.

Experiment 3: PK analysis. After a washout period, six mice from experiment 2 were administered 100 or 300 mg telaprevir kg^{-1} (n=3 each) BID at 19:00 and 9:00 h for 4 days. Serum samples were collected before dose administration, 4 (n=1) or 8 (n=2) h after administration of the second dose, and 5 h after every two doses were administered. After the final dose was administered, plasma for PK analysis was collected at 1 and 4 h. The mice were sacrificed at 8 h, and serum, plasma and liver samples were collected.

Experiment 4: dose dependence and PK/PD analysis. Thirty-six mice were infected with HCV and 13 survived for more than 13 weeks. The median survival time of this cohort was 81 days after infection. Twelve HCV-infected mice were randomized into three groups (A–C; n=4 each) and underwent two periods of BID dosing for 5 days, which were separated by 1-week washout periods. During the first period, the mice in groups A, B and C were administered 300 mg telaprevir kg^{-1}, 100 mg telaprevir kg^{-1} and vehicle,

respectively. Because two mice in group A and two mice in group C died before the second period, two remaining mice in group C and one back-up mouse were assigned to group A (n=2) and group B (n=1). During the second period, mice that received high or low doses were crossed over to the alternative treatment. Serum samples were collected before the first dose was administered and 5 h after every two doses were administered. Plasma samples were also collected at the same time on days 1, 3 and 5 in the first period and days 1, 3 and 4 in the second period. The mice were sacrificed 8 h after administration of the final dose, and serum, plasma and liver samples were collected.

Experiment 5: viral kinetics with BID dosing After infection of 45 mice, 12 HCV-infected mice maintained steady-state and high viral loads (1.2×10^6–8.5×10^7 copies ml^{-1}) for more than 6 months. The median survival time of this cohort was 131 days after infection. These mice were treated with 200 mg telaprevir kg^{-1} BID at 19:00 and 9:00 h for 3 days. The mice were divided into two groups and serum samples were collected just before the second dose was administered and 4 (n=6) or 8 (n=6) h after every two doses were administered.

Serum RNA extraction and HCV RNA quantification. HCV RNA was isolated from 10 µl serum under denaturing conditions using a SepaGene RV-R kit (Sanko Junyaku). The dried precipitates were dissolved in 10 µl diethylpyrocarbonate-treated water. Extracts were duplicated and assayed by quantitative real-time RT-PCR using TaqMan EZ RT-PCR core reagents (Applied Biosystems). Nucleotide positions of the probe and primer sets refer to HCV H77 strain (GenBank accession no. AF009606). The TaqMan probe 5′-6-FAM-CTGCGGAACCGGTGAGTACAC-BHQ-1-3′ (nt 148–168) was purchased from Biosearch Technologies, and the forward (5′-CGGGAGAGCCATAGTGG-3′; nt 130–146) and reverse (5′-AGTACCACAAGGCCTTTCG-3′; nt 272–290) primers were purchased from Sigma-Aldrich. The 25 µl RT-PCR mixture contained 0.2 nmol forward and reverse primers ml^{-1}, 0.3 nmol TaqMan probe ml^{-1} and 5 µl extracted RNA, and was monitored using a PRISM 7900HT sequence detection system (Applied Biosystems). The thermal profile was 2 min at 50 °C, 30 min at 60 °C for reverse transcription and 5 min at 95 °C, followed by 45 cycles of 20 s at 95 °C and 1 min at 62 °C. The HCV replicon I_{389}neo/NS3-3′/5.1 (Lohmann *et al.*, 1999) RNA was transcribed *in vitro* using a T7 RiboMax Express Large Scale RNA Production System (Promega) and purified twice using gel filtration. The concentration of this transcribed RNA was determined by absorbance at 260 nm and serially diluted 10-fold to prepare a standard curve for each assay.

Liver RNA extraction and HCV RNA quantification. A Wizard SV total RNA Isolation System (Promega) was used to obtain a DNase I-treated total RNA sample. The total RNA concentration was determined by absorbance at 260 nm. Total RNA samples were assayed by duplex real-time RT-PCR for relative quantification of HCV RNA using endogenous control gene expression of human β_2-microglobulin (hβ_2m; GenBank accession no. NM_004048), the TaqMan probe 5′-CAL Fluor Orange 560-AGTGGGATCG-AGACATGTAAGCAGCATCAT-BHQ-1-3′ (nt 401–430), and the forward and reverse primer set of 5′-TTGTCACAGCCCAA-GATAGTT-3′ (nt 379–399) and 5′-TGCGGCATCTTCAAACC-3′ (nt 434–450). To adjust the efficacy of PCR amplification of both target genes, the reaction condition was modified from the HCV single-probe assay. The temperature for extension was 60 °C, the concentration of the HCV probe was 0.24 nmol ml^{-1} and the reaction mixture contained the TaqMan probe/primer set for hβ_2m: 0.2 nmol primers ml^{-1} and 0.12 nmol TaqMan probe ml^{-1}. Because both target genes double after one cycle of PCR, a difference in Ct between HCV and hβ2m ($\Delta Ct = Ct_{HCV} - Ct_{h\beta2m}$) theoretically indicates a relative quantity of HCV RNA per control gene expression of $2^{-\Delta\Delta Ct}$.

Determination of drug concentration. Plasma and liver samples were analysed using chiral liquid chromatography followed by tandem mass spectrometry. After reconstitution, sample extracts were separated by normal-phase chromatography on a 2 × 250 mm Hypersil CPS-1 column (Thermo Hypersil-Keystone) with a mobile phase of heptane : acetone : methanol (82 : 17 : 1). Analyte concentrations were determined by turbo ion spray liquid chromatography/tandem mass spectrometry in the positive-ion mode. Analysis was performed at SRL or Mitsubishi Chemical Medience.

Statistical analysis. The HCV RNA level in serum was normalized by logarithmic conversion. Statistical analysis was performed with a mixed linear model using SAS (SAS Institute). Mean differences between two groups were evaluated with Student's t-test. The difference compared with vehicle control at each time point was evaluated by Dunnett's multiple comparisons test. Linear and non-linear regression analyses were performed using GraphPad Prism 5 (GraphPad Software).

Viral dynamics model analysis. The basic mathematical model for the analysis of HCV infection *in vivo*, which is a system of three ordinary differential equations for uninfected cells (T), productively infected cells (I) and free virus (V), has been reviewed elsewhere (Perelson & Ribeiro, 2008). Briefly, one of the three equations ($dV/dt = pI - cV$), where viral particles are produced at rate p per infected cell and cleared at rate c per virion, was solved. During treatment for 2–3 days, if one assumes that the number of I is approximately constant and equal to its pre-treatment value and that the viral level was at its set-point value (V_0), then $pI = cV_0$. Using this relationship in the equation $dV/dt = (1-\varepsilon)pI - cV$, where ε is the effectiveness in blocking virion production, yields $dV/dt = (1-\varepsilon)\,cV_0 - cV$, $V(0) = V_0$ with the solution $V(t) = V_0(1-\varepsilon+\varepsilon e^{-ct})$. Because the log change of viral load at time [$\log \Delta V(t)$] equals $\log V(t)/V_0$, the solved equation [$\log \Delta V(t) = \log(1-\varepsilon+\varepsilon e^{-ct})$] was fitted to the values obtained in this study via non-linear least-squares regression in order to estimate ε and c.

ACKNOWLEDGEMENTS

We thank Drs Ichimaro Yamada, Mitsubishi Tanabe Pharma Corporation, and Ann D Kwong, Gururaj Kalkeri, Susan Almquist, Steven M. Lyons and John Randle, Vertex Pharmaceuticals, for their thoughtful discussions. This work was supported in part by Grants-in-Aid for scientific research and development from the Ministry of Education, Sports, Culture and Technology and the Ministry of Health, Labour and Welfare, Japan.

REFERENCES

Boonstra, A., van der Laan, L. J. W., Vanwolleghem, T., Harry, L. A. & Janssen, H. L. A. (2009). Experimental models for hepatitis C viral infection. *Hepatology* **50**, 1646–1655.

Chang, M., Williams, O., Mittler, J., Quintanilla, A., Carithers, R. L., Jr, Perkins, J., Corey, L. & Gretch, D. R. (2003). Dynamics of hepatitis C virus replication in human liver. *Am J Pathol* **163**, 433–444.

Dahari, H., Feliu, A., Garcia-Retortillo, M., Forns, X. & Neumann, A. U. (2005). Second hepatitis C replication compartment indicated by viral dynamics during liver transplantation. *J Hepatol* **42**, 491–498.

Forestier, N., Reesink, H. W., Weegink, C. J., McNair, L., Kieffer, T. L., Chu, H.-M., Purdy, S., Jansen, P. L. M. & Zeuzem, S. (2007). Antiviral

activity of telaprevir (VX-950) and peginterferon alfa-2a in patients with hepatitis C. *Hepatology* **46**, 640–648.

Fried, M. W., Shiffman, M., Reddy, K. R., Smith, C., Marinos, G., Gonçales, F. L., Jr, Häussinger, D., Diago, M., Carosi, G. & other authors (2002). Peginterferon alfa-2a plus ribavirin for chronic hepatitis C virus infection. *N Engl J Med* **347**, 975–982.

Herrmann, E., Lee, J.-H., Marinos, G., Modi, M. & Zeuzem, S. (2003). Effect of ribavirin on hepatitis C viral kinetics in patients treated with pegylated interferon. *Hepatology* **37**, 1351–1358.

Hézode, C., Forestier, N., Dusheiko, G., Ferenci, P., Pol, S., Goeser, T., Bronowicki, M.,, Bourlière, J.-P., Gharakhanian, S. & other authors (2009). Telaprevir and peginterferon with or without ribavirin for chronic HCV infection. *N Engl J Med* **360**, 1839–1850.

Hiraga, N., Imamura, M., Tsuge, M., Noguchi, C., Takahashi, S., Iwao, E., Fujimoto, Y., Abe, H., Maekawa, T. & other authors (2007). Infection of human hepatocyte chimeric mouse with genetically engineered hepatitis C virus and its susceptibility to interferon. *FEBS Lett* **581**, 1983–1987.

Katoh, M., Sawada, T., Soeno, Y., Nakajima, M., Tateno, C., Yoshizato, K. & Yokoi, T. (2007). *In vivo* drug metabolism model for human cytochrome P450 enzyme using chimeric mice with humanized liver. *J Pharm Sci* **96**, 428–437.

Katoh, M., Tateno, C., Yoshizato, K. & Yokoi, T. (2008). Chimeric mice with humanized liver. *Toxicology* **246**, 9–17.

Kimura, T., Imamura, M., Hiraga, N., Hatakeyama, T., Miki, D., Noguchi, C., Mori, N., Tsuge, M., Takahashi, S. & other authors (2008). Establishment of an infectious genotype 1b hepatitis C virus clone in human hepatocyte chimeric mice. *J Gen Virol* **89**, 2108–2113.

Kneteman, N. M., Weiner, A. J., O'Connell, J., Collett, M., Gao, T., Aukerman, L., Kovelsky, R., Ni, Z.-J., Hashash, A. & other authors (2006). Anti-HCV therapies in chimeric *scid*-Alb/uPA mice parallel outcomes in human clinical application. *Hepatology* **43**, 1346–1353.

Kneteman, N. M., Howe, A. Y. M., Gao, T., Lewis, J., Pevear, D., Lund, G., Douglas, D., Mercer, D. F., Tyrrell, D. L. J. & other authors (2009). HCV796: a selective nonstructural protein 5B polymerase inhibitor with potent anti-hepatitis C virus activity *in vitro*, in mice with chimeric human livers, and in humans infected with hepatitis C virus. *Hepatology* **49**, 745–752.

Lauer, G. M. & Walker, B. D. (2001). Hepatitis C virus infection. *N Engl J Med* **345**, 41–52.

Liang, T. J., Rehermann, B., Seeff, L. B. & Hoofnagle, J. H. (2000). Pathogenesis, natural history, treatment and prevention of hepatitis C. *Ann Intern Med* **132**, 296–305.

Lindenbach, B. D., Meuleman, P., Ploss, A., Vanwolleghem, T., Syder, A. J., McKeating, J. A., Lanford, R. E., Feinstone, S. M., Major, M. E. & other authors (2006). Cell culture-grown hepatitis C virus is infectious *in vivo* and can be recultured *in vitro*. *Proc Natl Acad Sci U S A* **103**, 3805–3809.

Lohmann, V., Körner, F., Koch, J., Herian, U., Theilmann, L. & Bartenschlager, R. (1999). Replication of subgenomic hepatitis C virus RNAs in a hepatoma cell line. *Science* **285**, 110–113.

Manns, M. P., McHutchison, J. G., Gordon, S. C., Rustgi, V. K., Shiffman, M., Reindollar, R., Goodman, Z. D., Koury, K., Ling, M.-H. & other authors (2001). Peginterferon alfa-2b plus ribavirin compared with interferon alfa-2b plus ribavirin for initial treatment of chronic hepatitis C: a randomised trial. *Lancet* **358**, 958–965.

Manns, M. P., Foster, G. R., Rockstroh, J. K., Zeuzem, S., Zoulim, F. & Houghton, M. (2007). The way forward in HCV treatment – finding the right path. *Nat Rev Drug Discov* **6**, 991–1000.

McHutchison, J. G., Everson, G. T., Gordon, S. C., Jacobson, I. M., Sulkowski, M., Kauffman, R., McNair, L., Alam, J., Muir, A. J. & other authors (2009). Telaprevir with peginterferon and ribavirin for chronic HCV genotype 1 infection. *N Engl J Med* **360**, 1827–1838.

Mercer, D. F., Schiller, D. E., Elliott, J. F., Douglas, D. N., Hao, C., Rinfret, A., Addison, W. R., Fischer, K. P., Churchill, T. A. & other authors (2001). Hepatitis C virus replication in mice with chimeric human livers. *Nat Med* **7**, 927–933.

Neumann, A. U., Lam, N. P., Dahari, H., Gretch, D. R., Wiley, T. E., Layden, T. J. & Perelson, A. S. (1998). Hepatitis C viral dynamics *in vivo* and the antiviral efficacy of interferon-α therapy. *Science* **282**, 103–107.

Pawlotsky, J.-M., Dahari, H., Neumann, A. U., Hezode, C., Germanidis, G., Lonjon, I., Castera, L. & Dhumeaux, D. (2004). Antiviral action of ribavirin in chronic hepatitis C. *Gastroenterology* **126**, 703–714.

Pereira, A. A. & Jacobson, I. M. (2009). New and experimental therapies for HCV. *Nat Rev Gastroenterol Hepatol* **6**, 403–411.

Perelson, A. S. & Ribeiro, R. M. (2008). Estimating drug efficacy and viral dynamic parameters: HIV and HCV. *Stat Med* **27**, 4647–4657.

Perni, R. B., Almquist, S. J., Byrn, R. A., Chandorkar, G., Chaturvedi, P. R., Courtney, L. F., Decker, C. J., Dinehart, K., Gates, C. A. & other authors (2006). Preclinical profile of VX-950, a potent, selective, and orally bioavailable inhibitor of hepatitis C virus NS3-4A serine protease. *Antimicrob Agents Chemother* **50**, 899–909.

Powers, K. A., Ribeiro, R. M., Patel, K., Pianko, S., Nyberg, L., Pockros, P., Conrad, A. J., McHutchison, J. & Perelson, A. S. (2006). Kinetics of hepatitis C virus reinfection after liver transplantation. *Liver Transpl* **12**, 207–216.

Poynard, T., Yuen, M.-F., Ratziu, V. & Lai, C. L. (2003). Viral hepatitis C. *Lancet* **362**, 2095–2100.

Quinkert, D., Bartenschlager, R. & Lohmann, V. (2005). Quantitative analysis of the hepatitis C virus replication complex. *J Virol* **79**, 13594–13605.

Ramratnam, B., Bonhoeffer, S., Binley, J., Hurley, A., Zhang, L., Mittler, J. E., Minarkowitz, M., Moore, J. P., Perelson, A. S. & Ho, D. D. (1999). Rapid production and clearance of HIV-1 and hepatitis C virus assessed by large volume plasma apheresis. *Lancet* **354**, 1782–1785.

Reesink, H. W., Zeuzem, S., Weegink, C. J., Forestier, N., Vliet, A., van de Wetering de Rooij,, J., McNair, L., Purdy, S., Kauffman, R. & other authors (2006). Rapid decline of viral RNA in hepatitis C patients treated with VX-950: a phase Ib, placebo-controlled, randomized study. *Gastroenterology* **131**, 997–1002.

Sarrazin, C., Kieffer, T. L., Bartels, D., Hanzelka, B., Möh, U., Welker, M., Wincheringer, D., Zhou, Y., Chu, H.-M. & other authors (2007). Dynamic hepatitis C virus genotypic and phenotypic changes in patients treated with the protease inhibitor telaprevir. *Gastroenterology* **132**, 1767–1777.

Schiano, T. D., Gutierrez, J. A., Walewski, J. L., Fiel, M. I., Cheng, B., Bodenheimer, H., Jr, Thung, S. N., Chung, R. T., Schwartz, M. E. & other authors (2005). Accelerated hepatitis C virus kinetics but similar survival rates in recipients of liver grafts from living versus deceased donors. *Hepatology* **42**, 1420–1428.

Sherman, K. E., Fleischer, R., Laessig, K., Murray, J., Tauber, W. & Birnkrant, D. (2007). Development of novel agents for the treatment of chronic hepatitis C infection: summary of the FDA antiviral products advisory committee recommendations. *Hepatology* **46**, 2014–2020.

Talal, A. H., Ribeiro, R. M., Powers, K. A., Grace, M., Cullen, C., Hussain, M., Markatou, M. & Perelson, A. S. (2006). Pharmacodynamics of PEG-IFN α differentiate HIV/HCV coinfected sustained virological responders from nonresponders. *Hepatology* **43**, 943–953.

Tateno, C., Yoshizane, Y., Saito, N., Kataoka, M., Utoh, R., Yamasaki, C., Tachibana, A., Soeno, Y., Asahina, K. & other authors (2004). Near completely humanized liver in mice shows human-type metabolic responses to drugs. *Am J Pathol* **165**, 901–912.

Tsuge, M., Hiraga, N., Takaishi, H., Noguchi, C., Oga, H., Imamura, M., Takahashi, S., Iwao, E., Fujimoto, Y. & other authors (2005). Infection of human hepatocyte chimeric mouse with genetically engineered hepatitis B virus. *Hepatology* **42**, 1046–1054.

Vanwolleghem, T., Meuleman, P., Libbrecht, L., Roskams, T., De Vos, R. & Leroux-Roels, G. (2007). Ultra-rapid cardiotoxicity of the hepatitis C virus protease inhibitor BILN 2061 in the urokinase-type plasminogen activator mouse. *Gastroenterology* **133**, 1144–1155.

Vona, G., Tuveri, R., Delpuech, O., Vallet, A., Canioni, D., Ballardini, G., Trabut, J. B., Le Bail, B., Nalpas, B. & other authors (2004). Intrahepatic hepatitis C virus RNA quantification in microdissected hepatocytes. *J Hepatol* **40**, 682–688.

Wasley, A. & Alter, M. J. (2000). Epidemiology of hepatitis C: geographic differences and temporal trends. *Semin Liver Dis* **20**, 1–16.

Journal of General Virology (2010), 91, 1854–1864 DOI 10.1099/vir.0.019224-0

HBx protein is indispensable for development of viraemia in human hepatocyte chimeric mice

Masataka Tsuge,[1,2,3] Nobuhiko Hiraga,[1,3] Rie Akiyama,[1,3] Sachi Tanaka,[1,3] Miyuki Matsushita,[1,3] Fukiko Mitsui,[1,3] Hiromi Abe,[1,4] Shosuke Kitamura,[1,3] Tsuyoshi Hatakeyama,[1,3] Takashi Kimura,[1,3] Daiki Miki,[1,3] Nami Mori,[1,3] Michio Imamura,[1,3] Shoichi Takahashi,[1,3] C. Nelson Hayes[1,3] and Kazuaki Chayama[1,3,4]

Correspondence
Kazuaki Chayama
chayama@hiroshima-u.ac.jp

[1]Department of Medicine and Molecular Science, Division of Frontier Medical Science, Programs for Biomedical Research, Graduate School of Biomedical Sciences, Hiroshima University, Hiroshima, Japan

[2]Natural Science Center for Basic Research and Development, Hiroshima University, Hiroshima, Japan

[3]Liver Research Project Center, Hiroshima University, Hiroshima, Japan

[4]Laboratory for Liver Diseases, SNP Research Center, The Institute of Physical and Chemical Research (RIKEN), Yokohama, Japan

Received 15 December 2009
Accepted 5 March 2010

The non-structural X protein, HBx, of hepatitis B virus (HBV) is assumed to play an important role in HBV replication. Woodchuck hepatitis virus X protein is indispensable for virus replication, but the duck hepatitis B virus X protein is not. In this study, we investigated whether the HBx protein is indispensable for HBV replication *in vivo* using human hepatocyte chimeric mice. HBx-deficient (HBx-def) HBV was generated in HepG2 cells by transfection with an overlength HBV genome. Human hepatocyte chimeric mice were infected with HBx-def HBV with or without hepatic HBx expression by hydrodynamic injection of HBx expression plasmids. Serum virus levels and HBV sequences were determined with mice sera. The generated HBx-def HBV peaked in the sucrose density gradient at points equivalent to the generated HBV wild type and the virus in a patient's serum. HBx-def HBV-injected mice developed measurable viraemia only in continuously HBx-expressed liver. HBV DNA in the mouse serum increased up to 9 $\log_{10}$ copies ml^{-1} and the viraemia persisted for more than 2 months. Strikingly, all revertant viruses had nucleotide substitutions that enabled the virus to produce the HBx protein. It was concluded that the HBx protein is indispensable for HBV replication and could be a target for antiviral therapy.

INTRODUCTION

Chronic hepatitis B virus (HBV) infection is associated with the development of virus-related liver diseases, including chronic hepatitis, liver cirrhosis and hepatocellular carcinoma (HCC). HBV is a member of the family *Hepadnaviridae*, which consists of hepatotropic, small DNA viruses that infect their respective animal hosts (Ando *et al.*, 1999; Ganem & Schneider, 2001; Raney & McLachlan, 1991). HBV particles contain a 3.2 kb partially double-stranded circular DNA genome encoding four open reading frames (ORFs). The preS/S, pre-core/core, polymerase/reverse transcriptase and non-structural X protein (HBx) mRNAs are transcribed from each of the four ORFs (Seeger & Mason, 2000; Tang *et al.*, 2001). Although previous works have demonstrated that HBx protein is necessary for maximal HBV replication in cultured cells (Bouchard *et al.*, 2001; Keasler *et al.*, 2007; Leupin *et al.*, 2005; Tang *et al.*, 2005) and in mouse hepatocytes (Keasler *et al.*, 2007), the precise function of HBx in the virus life cycle remains poorly defined in human hepatocytes under physiological conditions because there is no natural infection–replication system available. Accordingly, all previous work has been done using hepatocarcinoma cell lines with transfection or mouse hepatocytes with hydrodynamic injection. Analysis of HBx under physiological conditions will provide more accurate information for the function of the HBx protein.

The nucleotide and amino acid sequences of the X genes are well-conserved among all mammalian hepadnaviruses. Expression of HBx protein in hepatocytes has been reported

The GenBank/EMBL/DDBJ accession number for the nucleotide sequence of the HBV genome cloned into plasmid pTRE-HB-wt is AB206817.